

ADA 027300

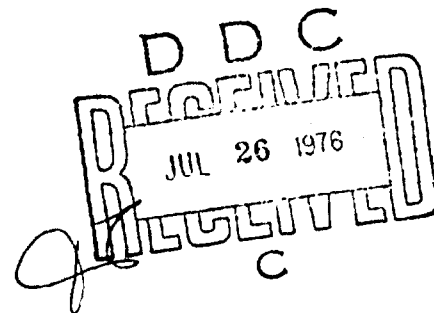
RADC-TR-76-169
IN-HOUSE REPORT
MAY 1976



Effect of Multipath on the Height-Finding Capabilities of a Fixed-Reflector Radar System Part 1: Analysis

RONALD L. FANTE
PETER R. FRANCHI
RICHARD L. TAYLOR

11H



Approved for public release; distribution unlimited.

ROME AIR DEVELOPMENT CENTER
AIR FORCE SYSTEMS COMMAND
GRIFFISS AIR FORCE BASE, NEW YORK 13441

PUBLICATION REVIEW

This report has been reviewed by the RADC Information Office (OI) and is releasable to the National Technical Information Service (NTIS). At NTIS it will be releasable to the general public, including foreign nations.

APPROVED:

Ronald L. Fante

RONALD L. FANTE
Acting Chief, ETEP

APPROVED:

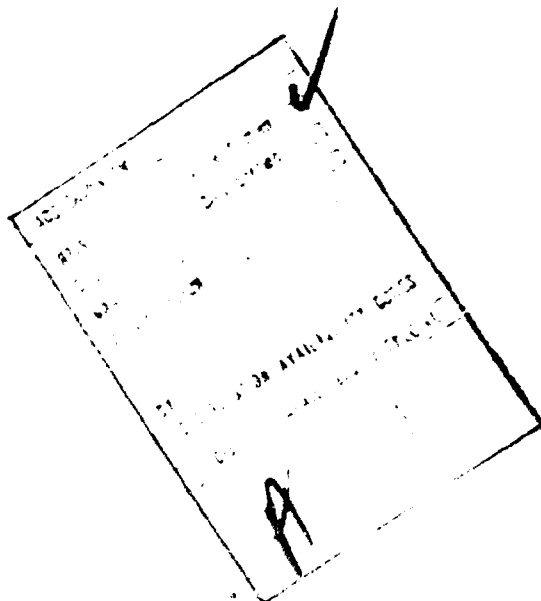
Carlyle J. Sletten

CARLYLE J. SLETTEN
Chief, Electromagnetic Sciences Division

FOR THE COMMANDER:

John P. Huse

Plans Office



*MISSION
of
Rome Air Development Center*

RADC plans and conducts research, exploratory and advanced development programs in command, control, and communications (C³) activities, and in the C³ areas of information sciences and intelligence. The principal technical mission areas are communications, electromagnetic guidance and control, surveillance of ground and aerospace objects, intelligence data collection and handling, information system technology, ionospheric propagation, solid state sciences, microwave physics and electronic reliability, maintainability and compatibility.



Printed by
United States Air Force
Harris AFB, Miss. 01731

Unclassified

SECURITY CLASSIFICATION OF THIS PAGE (When Data Entered)

REPORT DOCUMENTATION PAGE		READ INSTRUCTIONS BEFORE COMPLETING FORM
1. REPORT NUMBER RADC-TR-76-169	2. GOVT ACCESSION NO.	3. RECIPIENT'S CATALOG NUMBER
4. TITLE (and Subtitle) EFFECT OF MULTIPATH ON THE HEIGHT- FINDING CAPABILITIES OF A FIXED- REFLECTOR RADAR SYSTEM, PART I. ANALYSIS	5. TYPE OF REPORT & PERIOD COVERED In-House	
6. AUTHOR(s) Ronald L. Fante, Peter R. Franchi Richard L. Taylor	6. PERFORMING ORG. REPORT NUMBER	
7. PERFORMING ORGANIZATION NAME AND ADDRESS Deputy for Electronic Technology (RADC/ETEP) Hanscom AFB Massachusetts 01731	8. CONTRACT OR GRANT NUMBER(s)	
11. CONTROLLING OFFICE NAME AND ADDRESS Deputy for Electronic Technology (RADC/ETEP) Hanscom AFB Massachusetts 01731	10. PROGRAM ELEMENT, PROJECT, TASK AREA & WORK UNIT NUMBERS 21530201 62802F 681300	
14. MONITORING AGENCY NAME & ADDRESS (if different from Controlling Office)	12. REPORT DATE May 76	
12 31p.	13. REPORT NUMBER 30	
16 AF-6813	15. SECURITY CLASS. (of this report) Unclassified	
17 681300	18a. DECLASSIFICATION/DOWNGRADING SCHEDULE	
18. DISTRIBUTION STATEMENT (of this Report) Approved for public release; distribution unlimited.		
19. SUPPLEMENTARY NOTES		
20. KEY WORDS (Continue on reverse side if necessary and identify by block number) Radars Reflector antennas Multipath Monopulse		
20. ABSTRACT (Continue on reverse side if necessary and identify by block number) We have derived analytical expressions for the radiation pattern of a fixed reflector antenna on which there are two or more field horns operated in a monopulse mode to obtain target altitude information. We have obtained results for the radiation pattern of an arbitrary reflector located at an arbitrary height above the earth, and fed by horns which may be located at an arbitrary position		

DDC
REF ID: A681300
JUL 26 1976
REGISTERED

DD FORM 1 JAN 73 1473 EDITION OF 1 NOV 68 IS OBSOLETE

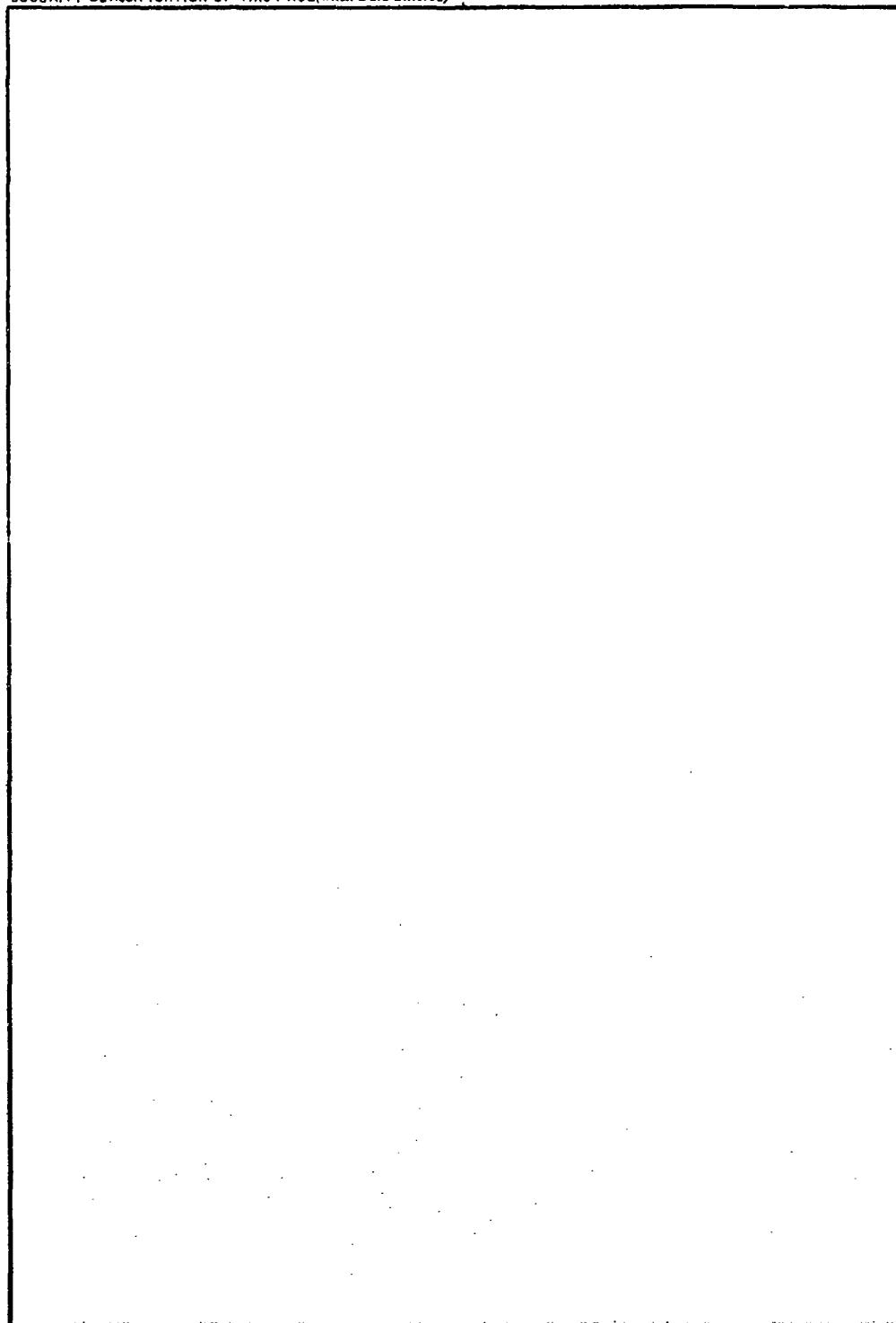
Unclassified

SECURITY CLASSIFICATION OF THIS PAGE (When Data Entered)

309050

45

SECURITY CLASSIFICATION OF THIS PAGE(When Data Entered)



SECURITY CLASSIFICATION OF THIS PAGE(When Data Entered)

Contents

1. INTRODUCTION	5
2. ELEMENT PATTERN (NO EARTH - THAT IS, VACUUM)	5
3. MULTIPATH EFFECTS	12
4. SYMMETRIC REFLECTOR AND HORN PATTERNS	21
5. FURTHER SIMPLIFICATION	25
6. ERROR IN ALTITUDE DUE TO MULTIPATH	26

Illustrations

1. Monopulse Operation of the Reflector Antenna	6
2. Assumed Reflector Geometry	7
3. Horn Radiation Coordinate System	9
4. Cross-Sectional View of Reflector-Horn Geometry	9
5. Geometry Used for Calculating the Multipath Effects	13
6. Projection of $z = f(x, y)$ onto the x-y Plane	22
7. Limiting Case of Grazing Incidence	25
8a. Plot of Output Voltage V Versus Target Altitude h in the Absence of Multipath, Showing How Measurement Error ΔV Leads to Altitude Error Δh	27
8b. Typical Plot of Altitude Error When Multipath is Absent	27

Illustrations

- | | |
|---|----|
| 9a. Plot of Output Voltage V_M Versus h When Multipath is Included | 29 |
| 9b. An Indication of How ΔV_M can be Used to Get Airplane Height Error Δh | 29 |
| 10. Typical Plots of Maximum Altitude Error Versus (a) Airplane Altitude and (b) Airplane Range | 30 |

Effect of Multipath on the Height-Finding Capabilites of a Fixed-Reflector Radar System Part I: Analysis

1. INTRODUCTION

In this report, we present the analytical methods for determining the error (due to multipath) in the altitude measuring capability of a reflector radar system operating in a monopulse mode. In particular, we will study the case of a fixed reflector antenna on which there are two separate horns in the focal region, with the horn output processed (see Figure 1) in such a fashion as to give altitude

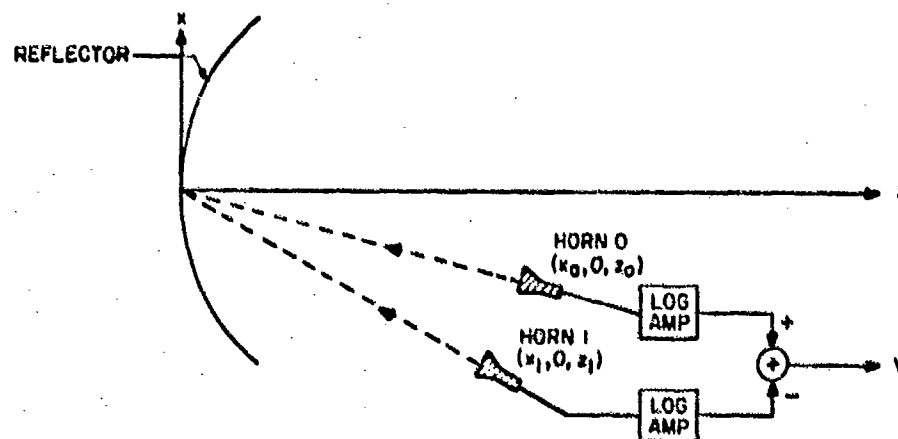


Figure 1. Monopulse Operation of the Reflector Antenna

(Received for publication 18 May 1976)

information. The analysis we will present here is valid for an arbitrary reflector located at an arbitrary height above the earth and for an arbitrary location of the two feed horns in the focal plane. In part II of this study, we will apply the results developed here to specific radar systems.

2. ELEMENT PATTERN (NO EARTH - THAT IS, VACUUM)

In the Physical Optics Approximation (reflector much larger than wavelength) the magnetic field scattered by a perfectly reflecting surface S is (see Silver¹)

$$\underline{H}_s = -\frac{1}{2\pi} \iint_S dS (\hat{n} \times \underline{H}_i) \times \nabla \left(\frac{e^{-ikR}}{R} \right) \quad (1)$$

where R is the distance from a point in dS on the surface S to the observation point, \hat{n} is the unit normal to the reflecting surface, and \underline{H} is the incident magnetic field from the primary source (horn antenna). Consider the system in Figure 2. The reflector surface is described by the arbitrary function

$$z = f(x, y) \quad (2)$$

The surface integral in Eq. (1) can now be written in terms of the projection of the reflector onto some plane, as shown in Figure 2. If we denote the projected area as S_0 , then (since $dS = dx dy [1 + (\partial f/\partial x)^2 + (\partial f/\partial y)^2]^{1/2}$)

$$\underline{H}_s = -\frac{1}{2\pi} \iint_{S_0} dx dy \left[1 + \left(\frac{\partial f}{\partial x} \right)^2 + \left(\frac{\partial f}{\partial y} \right)^2 \right]^{1/2} (\hat{n} \times \underline{H}_i) \times \nabla \left(\frac{e^{-ikR}}{R} \right) \quad (3)$$

1. Silver, S. (1965) Microwave Antenna Theory and Design, Dover Publications, Inc., New York.
2. Kaplan, W. (1953) Advanced Calculus, Addison-Wesley, Publishing Co., Inc., Cambridge, Massachusetts.

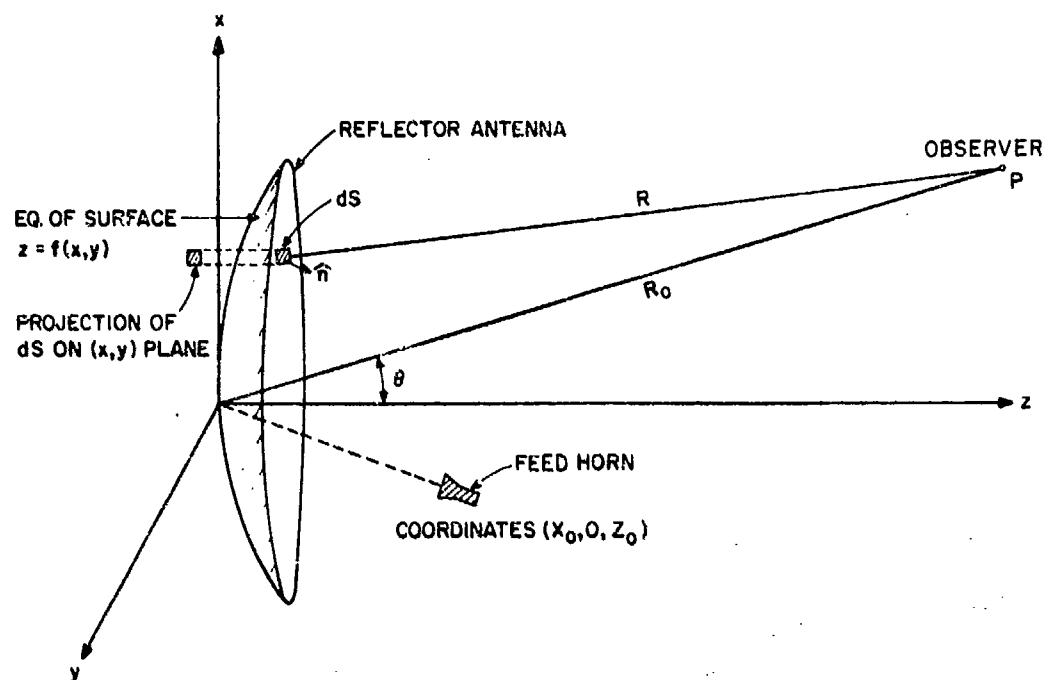


Figure 2. Assumed Reflector Geometry. Azimuthal angle ϕ of observer is not shown

where

$$\hat{n} = \frac{\hat{z} - \left(\frac{\partial f}{\partial x}\right) \hat{x} - \left(\frac{\partial f}{\partial y}\right) \hat{y}}{\left[1 + \left(\frac{\partial f}{\partial x}\right)^2 + \left(\frac{\partial f}{\partial y}\right)^2\right]^{1/2}} \quad (4)$$

and \hat{x} , \hat{y} and \hat{z} are unit vectors along the x , y , z axes. Now

$$\begin{aligned} \nabla \left(\frac{e^{-ikR}}{R} \right) &= -\frac{ik}{R} e^{-ikR} (\nabla R) - \frac{e^{-ikR}}{R^2} (\nabla R) \\ &\approx -\frac{ik}{R_0} (\hat{x} \sin \theta \cos \phi + \hat{y} \sin \theta \sin \phi + \hat{z} \cos \theta) \\ &\quad \cdot \exp[-ik(R_0 - x \sin \theta \cos \phi - y \sin \theta \sin \phi - z \cos \theta)] \end{aligned} \quad (5)$$

in the Fraunhofer Zone. If we use (4) and (5) in (3) we get

$$\begin{aligned} \underline{H}_s = \frac{ik}{2\pi R_0} \iint_{S_0} dx dy & \left[\left(\hat{z} - \hat{x} \frac{\partial f}{\partial x} - \hat{y} \frac{\partial f}{\partial y} \right) \times \underline{H}_i \right] \\ & \times [\hat{x} \sin \theta \cos \phi + \hat{y} \sin \theta \sin \phi + \hat{z} \cos \theta] \\ & \cdot \exp \{-ik R_0 + ik(x \sin \theta \cos \phi + y \sin \theta \sin \phi + z \cos \theta)\} \end{aligned} \quad (6)$$

Note that in (6), the quantity $z = f(x, y)$. From practical reflectors, quite often $z = f(x, y)$ can be expressed as $z = \alpha(x) + \beta(x)y^2 + \gamma(x)y^4$. The problem now is to calculate the incident magnetic field \underline{H}_i due to the horn antenna. For the horn antenna representation, consider Figure 3. We characterize the horn radiation pattern by the electric field distribution (horizontal polarization)

$$\underline{E}_i = \hat{\phi}_0 F(\psi_0) g(\eta_0) \frac{e^{-iks_0}}{s_0} \quad (7)$$

where $\hat{\phi}_0$ is the unit vector shown in Figure 3 and can be written as

$$\hat{\phi}_0 = \hat{y}' \cos \eta_0 - \hat{z}' \sin \eta_0 \quad (8)$$

and \hat{y}' and \hat{z}' are unit vectors along y' and z' . Also s_0 is shown on Figure 4 and is given by

$$s_0 = [(x - x_0)^2 + y^2 + (z - z_0)^2]^{1/2} \quad (9)$$

From the geometry in Figure 4, it can be seen that

$$\psi_0 = \tan^{-1} \left(\frac{x - x_0}{z_0 - z} \right) + \tan^{-1} \left(\frac{y}{z_0 - z} \right) \quad (10)$$

$$\eta_0 = \tan^{-1} \left(\frac{y}{z_0 - z} \right) \quad (11)$$

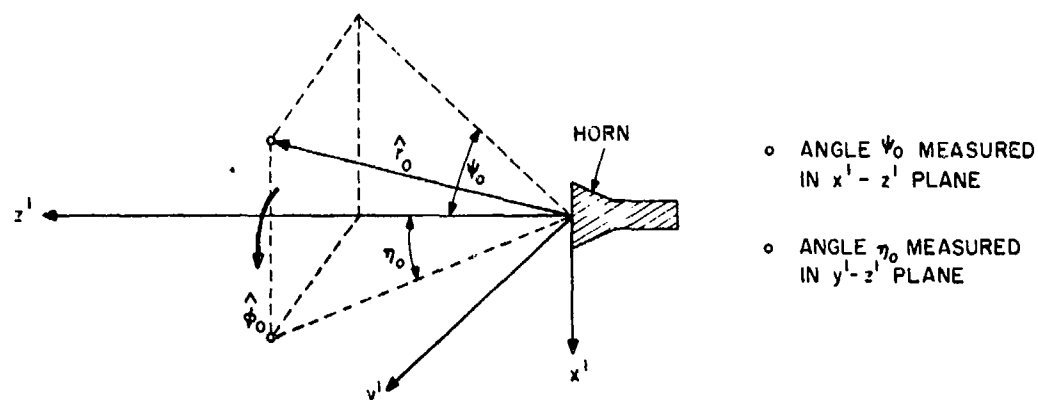


Figure 3. Horn Radiation Coordinate System

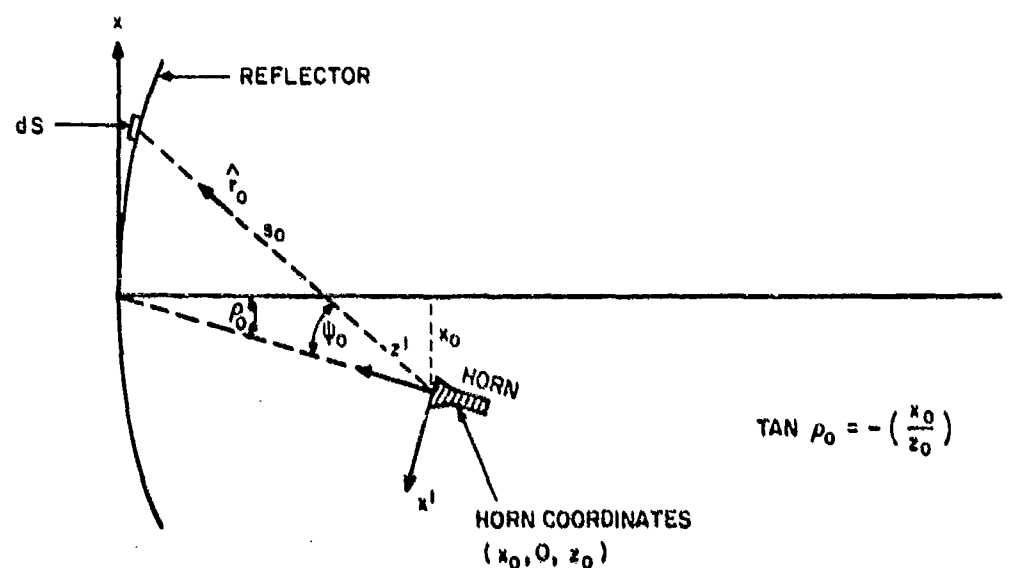


Figure 4. Cross-Sectional View of Reflector-Horn Geometry

where \tan^{-1} is of modulo $\left(-\frac{\pi}{2}, \frac{\pi}{2}\right)$. From Eq. (7), we see that we are assuming \underline{E}_i is horizontally polarized and can be represented as the product of the arbitrary functions (that is, they can be anything we want them to be) $F(\psi_0)$ and $g(\eta_0)$. Note that s_0 , ψ_0 and η_0 all depend on x and y , as is evident from Eqs. (9) to (11).

We next have to calculate the incident magnetic field. This can be obtained from (7) via

$$\underline{H}_i = Y_o \hat{r}_o \times \underline{E}_i \quad (12)$$

where \hat{r}_o is the unit vector shown in Figures 2 and 3, and Y_o is the characteristic admittance of vacuum. In the (x', y', z') coordinate system shown in Figure 2, we get

$$\hat{r}_o = \frac{-\hat{x}' \sin \psi_o \cos \eta_o + \hat{y}' \sin \eta_o \cos \psi_o + \hat{z}' \cos \psi_o \cos \eta_o}{[\cos^2 \eta_o + \sin^2 \eta_o \cos^2 \psi_o]^{1/2}}, \quad (13)$$

so that in the (x', y', z') coordinate system

$$\begin{aligned} \underline{H}_i &= Y_o F(\psi_o) g(\eta_o) \frac{e^{-iks_o}}{s_o} (\hat{r}_o \times \hat{\phi}_o) \\ &= \hat{h}_o Y_o F(\psi_o) g(\eta_o) \frac{e^{-iks_o}}{s_o}, \end{aligned} \quad (14)$$

where

$$\begin{aligned} \hat{h}_o &= \frac{\hat{x}' \cos \psi_o + \hat{y}' \sin \psi_o \cos \eta_o \sin \eta_o + \hat{z}' \sin \psi_o \cos^2 \eta_o}{\Delta_o}, \\ \Delta_o &= [\cos^2 \eta_o + \sin^2 \eta_o \cos^2 \psi_o]^{1/2}. \end{aligned} \quad (15)$$

Upon transforming to the (x, y, z) coordinate system used in Figures 2 and 4 we have

$$\hat{h}_o = \alpha_o \hat{x} + \beta_o \hat{y} + \gamma_o \hat{z}, \quad (16)$$

where

$$\alpha_o = \frac{\cos \psi_o \cos \rho_o - \sin \psi_o \cos^2 \eta_o \sin \rho_o}{\Delta_o}, \quad (17)$$

$$\beta_0 = -\frac{\sin \psi_0 \cos \eta_0 \sin \eta_0}{\Delta_0} \quad (18)$$

$$\gamma_0 = \frac{\cos \psi_0 \sin \rho_0 + \cos \rho_0 \sin \psi_0 \cos^2 \eta_0}{\Delta_0} \quad (19)$$

$$\rho_0 = -\tan^{-1} \left(\frac{x_0}{z_0} \right) \quad (20)$$

If we now use Eq. (16) in (14) and then use that result in (6), we get

$$\underline{H}_s = \frac{ik Y_0 e^{-ikR_0}}{2\pi R_0} \iint_{S_0} dx dy \frac{F(\psi_0) g(\eta_0)}{s_0} \{A_0 \hat{x} + B_0 \hat{y} + C_0 \hat{z}\} e^{-ik(s_0 - x \sin \theta \cos \phi - y \sin \theta \sin \phi - z \cos \theta)} \quad (21)$$

where

$$A_0 = \cos \theta \left(\alpha_0 + \gamma_0 \frac{\partial f}{\partial x} \right) - \sin \theta \sin \phi \left(\alpha_0 \frac{\partial f}{\partial y} - \beta_0 \frac{\partial f}{\partial x} \right) \quad (22)$$

$$B_0 = \cos \theta \left(\beta_0 + \gamma_0 \frac{\partial f}{\partial y} \right) + \sin \theta \cos \phi \left(\alpha_0 \frac{\partial f}{\partial y} - \beta_0 \frac{\partial f}{\partial x} \right) \quad (23)$$

$$C_0 = -\sin \theta \sin \phi \left(\beta_0 + \gamma_0 \frac{\partial f}{\partial y} \right) - \sin \theta \cos \phi \left(\alpha_0 + \gamma_0 \frac{\partial f}{\partial x} \right) \quad (24)$$

The radiated power pattern is proportional to

$$P_0(\theta, \phi) = R_0^2 \underline{E}_s \times \underline{H}_s^* = \frac{R_0^2}{Y_0} (\hat{n}_s \times \underline{H}_s) \times \underline{H}_s^* = \frac{R_0^2}{Y_0} \underline{H}_s \cdot \underline{H}_s^* \quad (25)$$

where \hat{n}_s is a unit vector in the direction of the observation point.

If we use Eq. (21) in (25), we get

$$\begin{aligned} \frac{4\pi^2 P_0(\theta, \phi)}{k^2 Y_0} = & \left| \iint_{S_0} dx dy \frac{F(\psi_0) g(\eta_0) A_0}{s_0} e^{-ikp_0} \right|^2 \\ & + \left| \iint_{S_0} dx dy \frac{F(\psi_0) g(\eta_0) B_0}{s_0} e^{-ikp_0} \right|^2 \\ & + \left| \iint_{S_0} dx dy \frac{F(\psi_0) g(\eta_0) C_0}{s_0} e^{-ikp_0} \right|^2, \end{aligned} \quad (26)$$

where

$$P_0 \equiv s_0 - x \sin \theta \cos \phi - y \sin \theta \sin \phi - z \cos \theta. \quad (27)$$

3. MULTIPATH EFFECTS

When the reflector in Figure 1 is located above the earth, the field at P will consist not only of the direct component in Eq. (21), but also the multipath component scattered from the earth, as is indicated in Figure 5. In Figure 5 we have denoted the transmitter altitude as d , the airplane altitude as h , and the grazing angle of the multipath ray by ψ_2 . Also, a_e is the effective radius of the earth and is approximately equal to $4/3$ of the actual radius of the earth. We use a_e to account for the refraction by the earth's atmosphere. In calculating the multipath field we will, for simplicity, restrict our calculations to the $\phi = 0$ plane.

In order to calculate the multipath field, it is first necessary to obtain expressions for the location r_2 of the reflection point on the earth, and also for the grazing angle ψ_2 . Using Section 2.13 in Kerr³ we have

$$(a) \quad h \geq d$$

$$r_1 = \frac{r}{2} + p \cos \left(\frac{\phi + \pi}{3} \right). \quad (28)$$

3. Kerr, Donald (1965) Propagation of Short Radio Waves, Dover Publications, Inc., New York.

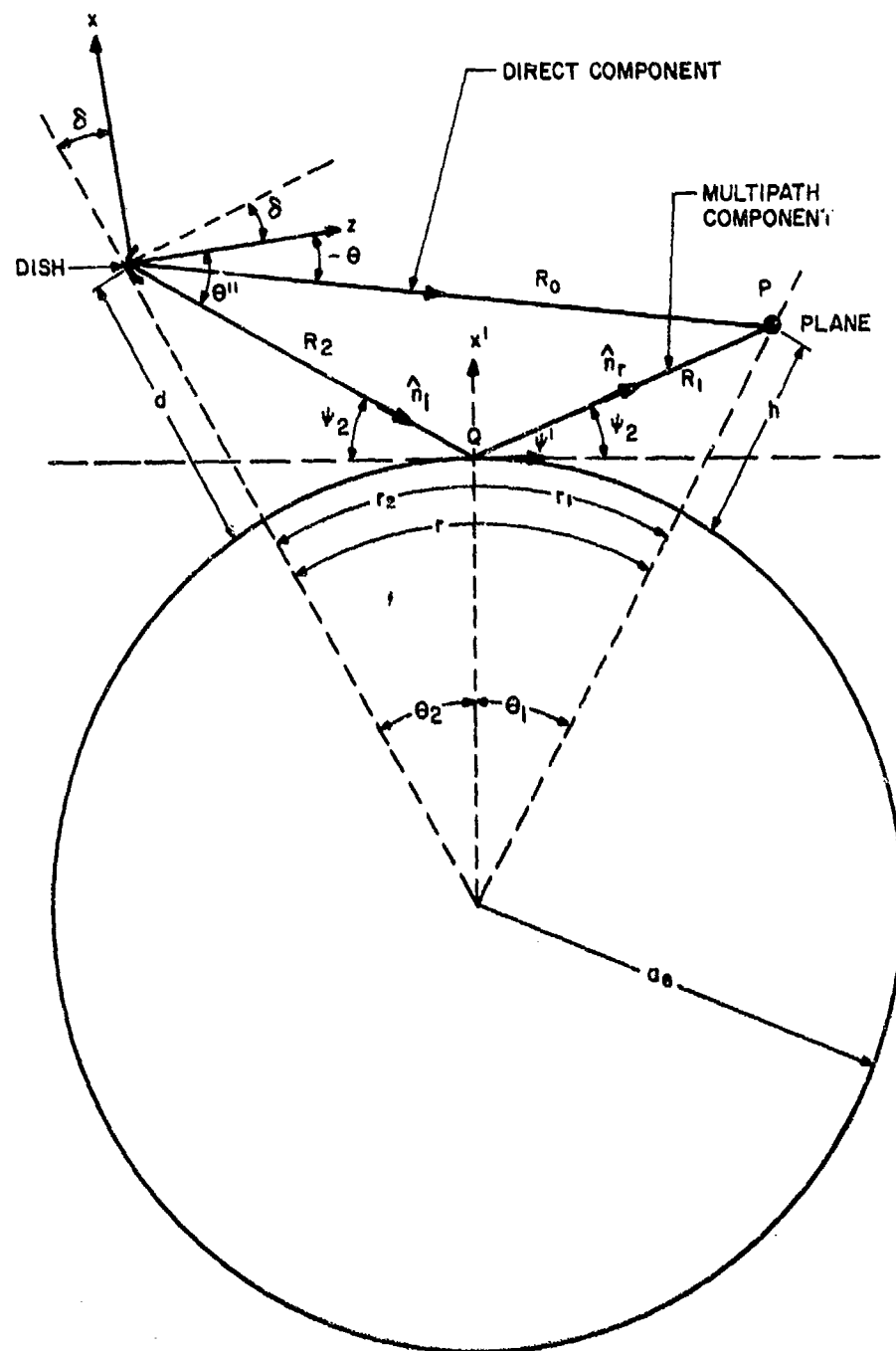


Figure 5. Geometry Used for Calculating the Multipath Effects

where

$$p = \frac{2}{(3)^{1/2}} \left[a_e(h+d) + \left(\frac{r}{2}\right)^2 \right]^{1/2},$$

$$\Phi = \cos^{-1} \left[\frac{2a_e(h-d)r}{p^3} \right],$$

$$D = \left[1 + \frac{4S_1^2 S_2 T}{S(1-S_1^2)(1+T)} \right]^{-1/2}, \quad (29)$$

$$\psi_2 = \tan^{-1} \left\{ \left(\frac{h+d}{r}\right) \left[\frac{(1-S_1^2) + T^2(1-S_2^2)}{1+T^2} \right] \right\}, \quad (30)$$

$$S_1 = \frac{r_1}{(2a_e h)^{1/2}}, \quad S_2 = \frac{r_2}{(2a_e d)^{1/2}},$$

$$S = \frac{r}{(2a_e h)^{1/2} + (2a_e d)^{1/2}}, \quad T = \left(\frac{d}{h}\right)^{1/2},$$

$$r = r_1 + r_2.$$

For the dish higher than the airplane, we have

(b) $d > h$

$$r_2 = \frac{r}{2} + p \cos \left(\frac{\Phi + \pi}{3} \right), \quad (31)$$

$$p = \frac{2}{(3)^{1/2}} \left[a_e(h+d) + \left(\frac{r}{2}\right)^2 \right]^{1/2},$$

$$\Phi = \cos^{-1} \left[\frac{2a_e(d-h)r}{p^3} \right],$$

$$\psi_2 = \tan^{-1} \left\{ \left(\frac{h+d}{r}\right) \left[\frac{(1-S_1^2) + T^2(1-S_2^2)}{1+T^2} \right] \right\}. \quad (32)$$

$$D = \left[1 + \frac{4 S_1^2 S_2 T}{S(1 - S_1^2)(1 + T)} \right]^{-1/2} \quad (33)$$

$$S_1 = \frac{r_2}{(2a_e d)^{1/2}} \quad , \quad S_2 = \frac{r_1}{(2a_e h)^{1/2}} \quad ,$$

$$T = \left(\frac{h}{d} \right)^{1/2} \quad ,$$

$$r_1 = r - r_2 \quad .$$

Now from Figure 5, we see that

$$\theta_2 = \frac{r_2}{a_e} \quad , \quad (34a)$$

$$\theta_1 = \frac{r_1}{a_e} \quad , \quad (34b)$$

$$R_2 = [(a_e + d)^2 + a_e^2 - 2a_e(a_e + d) \cos \theta_2]^{1/2} \quad , \quad (35a)$$

$$R_1 = [(a_e + h)^2 + a_e^2 - 2a_e(a_e + h) \cos \theta_1]^{1/2} \quad . \quad (35b)$$

Also

$$\theta'' = \sin^{-1} \left(\frac{(a_e + d)^2 + R_2^2 - a_e^2}{2R_2(a_e + d)} \right) - \delta \quad . \quad (36)$$

We can next write the incident magnetic field at the reflection point Q (see Figure 5) as

$$\underline{H}(Q) = \frac{ik Y_0 e^{-ikR_2}}{R_2} \iint_{S_0} dx dy \frac{F(\psi_0) g(\eta_0)}{s_0} e^{-ik(s_0 + xsin\theta'' - zcos\theta'')} \quad (37)$$

$$\cdot (A_0'' \hat{x} + B_0'' \hat{y} + C_0'' \hat{z})$$

$$= H_x \hat{x} + H_y \hat{y} + H_z \hat{z} , \quad (37)$$

where

$$A''_0 = \cos \theta'' \left(\alpha_0 + \gamma_0 \frac{\partial f}{\partial x} \right) , \quad (38)$$

$$B''_0 = \cos \theta'' \left(\beta_0 + \gamma_0 \frac{\partial f}{\partial y} \right) - \sin \theta'' \left(\alpha_0 \frac{\partial f}{\partial y} - \beta_0 \frac{\partial f}{\partial x} \right) , \quad (39)$$

$$C''_0 = \sin \theta'' \left(\alpha_0 + \gamma_0 \frac{\partial f}{\partial x} \right) . \quad (40)$$

Now we transform the fields to the prime coordinate system, which is shown in Figure 5. We have the unit vector relationships

$$\hat{x} = \hat{x}' \cos (\theta_2 - \delta) - \hat{z}' \sin (\theta_2 - \delta) , \quad (41)$$

and

$$\hat{z} = \hat{z}' \cos (\theta_2 - \delta) + \hat{x}' \sin (\theta_2 - \delta) . \quad (42)$$

Also, the unit vectors \underline{n}_I and \underline{n}_R directed along the incident and reflected wave vector are

$$\begin{aligned} \underline{n}_I &= \hat{z}' \cos \psi_2 - \hat{x}' \sin \psi_2 , \\ \underline{n}_R &= \hat{z}' \cos \psi_2 + \hat{x}' \sin \psi_2 . \end{aligned} \quad (43)$$

Therefore, in the primed coordinate system

$$\begin{aligned} \underline{H}_I(P) &= H_x \{ \hat{x}' \cos (\theta_2 - \delta) - \hat{z}' \sin (\theta_2 - \delta) \} + H_y \hat{y}' \\ &\quad + H_z \{ \hat{z}' \cos (\theta_2 - \delta) + \hat{x}' \sin (\theta_2 - \delta) \} \\ &= \hat{x}' [H_x \cos (\theta_2 - \delta) + H_z \sin (\theta_2 - \delta)] + \hat{y}' H_y \\ &\quad + \hat{z}' [H_z \cos (\theta_2 - \delta) - H_x \sin (\theta_2 - \delta)] , \end{aligned} \quad (44)$$

and the incident \underline{E} field is

$$\begin{aligned} Y_0 \underline{E}_i(P) = & \hat{x}' H_y \cos \psi_2 - y' [H_x \cos (\psi_2 + \theta_2 - \delta) + H_z \sin (\psi_2 + \theta_2 - \delta)] \\ & + \hat{z}' H_y \sin \psi_2 . \end{aligned} \quad (45)$$

Now at the reflection point we have that* (for perfect conductivity or very small grazing angles)

$$(E_R)_{z'} = - (E_i)_{z'}$$

$$(E_R)_{y'} = - (E_i)_{y'}$$

$$(E_R)_{x'} = (E_i)_{x'}$$

$(E_R)_{x'}$ means the x' component of \underline{E}_R . Therefore

$$\begin{aligned} \frac{Y_0}{|\rho(\psi_2)|D} \underline{E}_R = & \hat{x}' H_y \cos \psi_2 + \hat{y}' \{ H_x \cos (\psi_2 + \theta_2 - \delta) + H_z \sin (\psi_2 + \theta_2 - \delta) \} \\ & - \hat{z}' H_y \sin \psi_2 \end{aligned} \quad (46)$$

where $|\rho(\psi_2)| \simeq 1$ is the reflection coefficient at Q, and D is the spherical dispersion factor defined in Eqs. (29) and (33). Now, the reflected magnetic field is

$$\underline{H}_R = Y_0 (\underline{n}_R \times \underline{E}_R) ,$$

or

$$\begin{aligned} \frac{\underline{H}_R}{D} = & \hat{x}' [- H_x \cos \psi_2 \cos (\psi_2 + \theta_2 - \delta) - H_z \cos \psi_2 \sin (\psi_2 + \theta_2 - \delta)] \\ & + \hat{y}' H_y \\ & + \hat{z}' [H_x \sin \psi_2 \cos (\psi_2 + \theta_2 - \delta) + H_z \sin \psi_2 \sin (\psi_2 + \theta_2 - \delta)] . \end{aligned} \quad (47)$$

*We will assume that the reflection is specular. This ignores the effect of diffuse reflection, and is valid provided the height σ of the surface bumps are such that $\sigma < \frac{\lambda}{8 \sin \psi_2}$, where λ = signal wavelength.

We now use Eq. (42) to express \underline{H}_R in the (x, y, z) coordinate system

$$\begin{aligned} \frac{\underline{H}_R}{D} = & -\hat{x} \cos(\psi_2 - \theta_2 + \delta) [H_x \cos(\psi_2 + \theta_2 - \delta) + H_z \sin(\psi_2 + \theta_2 - \delta)] \\ & + \hat{y} H_y \\ & + \hat{z} \sin(\psi_2 - \theta_2 + \delta) [H_x \cos(\psi_2 + \theta_2 - \delta) + H_z \sin(\psi_2 + \theta_2 - \delta)] \end{aligned} \quad (48)$$

Therefore, the multipath magnetic field at the airplane location is

$$\begin{aligned} \underline{H}_R \approx & \frac{ik Y_0 D e^{-ikR_3}}{R_0} \iint_{S_0} dx dy \frac{F(\psi_0) g(\eta_0)}{s_0} e^{-ik(s_0 + x \sin \theta'' - z \cos \theta'')} \\ & \cdot \{A_0''' \hat{x} + B_0''' \hat{y} + C_0''' \hat{z}\} \end{aligned} \quad (49)$$

where

$$R_3 = R_1 + R_2$$

and

$$A_0''' = -\left(\alpha_0 + \gamma_0 \frac{\partial f}{\partial x}\right) \cos(\psi_2 - \theta_2 + \delta) \cos(\psi_2 + \theta_2 - \delta - \theta'') \quad (50)$$

$$B_0''' = \cos \theta'' \left(\beta_0 + \gamma_0 \frac{\partial f}{\partial y}\right) - \sin \theta'' \left(\alpha_0 \frac{\partial f}{\partial y} - \beta_0 \frac{\partial f}{\partial x}\right) \quad (51)$$

$$C_0''' = \left(\alpha_0 + \gamma_0 \frac{\partial f}{\partial x}\right) \sin(\psi_2 - \theta_2 + \delta) \cos(\psi_2 + \theta_2 - \delta - \theta'') \quad (52)$$

Now, from Figure 5 it is clear that

$$\left(\frac{\pi}{2} - \theta'' - \delta\right) + \theta_2 + \left(\frac{\pi}{2} + \psi_2\right) = \pi$$

or

$$\psi_2 + \theta_2 - \delta - \theta'' = 0 \quad (53)$$

Therefore

$$A_0''' = - \left(\alpha_0 + \gamma_0 \frac{\partial f}{\partial x} \right) \cos (\psi_2 - \theta_2 + \delta) , \quad (54)$$

$$B_0''' = \cos \theta'' \left(\beta_0 + \gamma_0 \frac{\partial f}{\partial y} \right) - \sin \theta'' \left(\alpha_0 \frac{\partial f}{\partial y} - \beta_0 \frac{\partial f}{\partial x} \right) , \quad (55)$$

$$C_0''' = \left(\alpha_0 + \gamma_0 \frac{\partial f}{\partial x} \right) \sin (\psi_2 - \theta_2 + \delta) . \quad (56)$$

We now obtain the total magnetic field at P by adding (21) and (49)

$$\begin{aligned} \underline{H}_{\text{TOTAL}}(P) = & \frac{ik y_0 e^{-ikR_0}}{2\pi R_0} \iint_{S_0} dx dy \frac{F(\psi_0) g(\eta_0)}{s_0} e^{-iks_0} \\ & \cdot \left\{ \hat{x} \left[A_0 e^{i\xi_1} + A_0''' v e^{-i\xi_4} \right] \right. \\ & + \hat{y} \left[B_0 e^{i\xi_1} + B_0''' v e^{-i\xi_4} \right] \\ & \left. + \hat{z} \left[C_0 e^{i\xi_1} + C_0''' v e^{-i\xi_4} \right] \right\} , \end{aligned} \quad (57)$$

where

$$\xi_1 = k(x \sin \theta + z \cos \theta) ,$$

$$\xi_4 = k(x \sin \theta'' - z \cos \theta'' + R_3 - R_0) ,$$

$$v = |\rho(\psi_2)| D \simeq D .$$

Therefore, the power pattern is (including multipath)

$$\begin{aligned} \frac{4\pi^2 P_{M0}(\theta)}{k^2 Y_0} = & \left| \iint_{S_0} dx dy \frac{F(\psi_0) g(\eta_0)}{s_0} e^{-iks_0} \left[A_0 e^{i\xi_1} + A_0''' v e^{-i\xi_4} \right] \right|^2 \\ & + \left| \iint_{S_0} dx dy \frac{F(\psi_0) g(\eta_0)}{s_0} e^{-iks_0} \left[B_0 e^{i\xi_1} + B_0''' v e^{-i\xi_4} \right] \right|^2 \\ & + \left| \iint_{S_0} dx dy \frac{F(\psi_0) g(\eta_0)}{s_0} e^{-iks_0} \left[C_0 e^{i\xi_1} + C_0''' v e^{-i\xi_4} \right] \right|^2 . \end{aligned} \quad (58)$$

We now relate θ and h . From Figure 5, we first calculate that

$$R_0^2 = (a_e + d)^2 + (a_e + h)^2 - 2(a_e + d)(a_e + h) \cos \theta_T . \quad (59)$$

$$\theta_T = \theta_1 + \theta_2 = \frac{r_1 + r_2}{a_e} = \frac{r}{a_e} . \quad (60)$$

Also, from Figure 5 we can relate θ and h via

$$(a_e + h)^2 = R_0^2 + (a_e + d)^2 - 2R_0(a_e + d) \cos (\pi/2 - \delta + \theta) . \quad (61)$$

Therefore

$$\theta(h) = \sin^{-1} \left\{ \frac{(a_e + h)^2 - (a_e + d)^2 - R_0^2}{2R_0(a_e + d)} \right\} + \delta . \quad (62)$$

Therefore, if we use Eq. (62), we can then use Eq. (58) to express P_{M0} as a function of the airplane altitude h rather than the angle θ .

For feed horn at (x_1, z_1) instead of (x_0, z_0) , we get for the power pattern including multipath

$$\begin{aligned}
\frac{4\pi^2 P_{M1}(\theta)}{k^2 Y_0} = & \left| \iint_{S_0} dx dy \frac{F(\psi_1) g(\eta_1)}{s_1} e^{-iks_1} \left[A_1 e^{i\xi_1} + A_1''' v e^{-i\xi_4} \right] \right|^2 \\
& + \left| \iint_{S_0} dx dy \frac{F(\psi_1) g(\eta_1)}{s_1} e^{-iks_1} \left[B_1 e^{i\xi_1} + B_1''' v e^{-i\xi_4} \right] \right|^2 \\
& + \left| \iint_{S_0} dx dy \frac{F(\psi_1) g(\eta_1)}{s_1} \left[C_1 e^{i\xi_1} + C_1''' v e^{-i\xi_4} \right] \right|^2 .
\end{aligned} \tag{63}$$

where

$$s_1 = [(x - x_1)^2 + y^2 + (z - z_1)^2]^{1/2} ,$$

$$\psi_1 = \tan^{-1} \left(\frac{x - x_1}{z_1 - z} \right) + \tan^{-1} \left(\frac{x_1}{z_1} \right) ,$$

$$\eta_1 = \tan^{-1} \left(\frac{y}{z_1 - z} \right) ,$$

$$A_1 = \left(\alpha_1 + \gamma_1 \frac{\partial f}{\partial x} \right) \cos \theta , \tag{64}$$

$$A_1''' = - \left(\alpha_1 + \gamma_1 \frac{\partial f}{\partial x} \right) \cos (\psi_2 - \theta_2 + \delta) , \tag{65}$$

$$C_1 = - \sin \theta \left(\alpha_1 + \gamma_1 \frac{\partial f}{\partial x} \right) , \tag{66}$$

$$C_1''' = \left(\alpha_1 + \gamma_1 \frac{\partial f}{\partial x} \right) \sin (\psi_2 - \theta_2 + \delta) , \tag{67}$$

etc .

4. SYMMETRIC REFLECTOR AND HORN PATTERNS

Let us now suppose that the reflector and the feed horn are symmetric in the y -direction. That is, for the reflector surface $z = f(x, y)$ we have

$$f(x, -y) = f(x, y) \quad .$$

Also, for the horn y-plane pattern we assume

$$g(-\eta_0) = g(\eta_0) \quad . \quad (68)$$

Then, we write Eq. (21) as (for $\phi = 0$ plane)

$$\begin{aligned} \left(\frac{2\pi R_0 e^{ikR_0}}{ikY_0} \right) H_s = & \int_{x_a}^{x_b} dx \int_{-y_a(x)}^0 dy \frac{F(\psi_0) g(\eta_0)}{s_0} e^{-ik(s_0 - x \sin \theta - z \cos \theta)} \\ & \cdot \{ \hat{x} A_0(x, y) + \hat{y} B_0(x, y) + \hat{z} C_0(x, y) \} \\ & + \int_{x_a}^{x_b} dx \int_0^{y_a(x)} dy \frac{F(\psi_0) g(\eta_0)}{s_0} e^{-ik(s_0 - x \sin \theta - z \cos \theta)} \\ & \cdot \{ \hat{x} A_0(x, y) + \hat{y} B_0(x, y) + \hat{z} C_0(x, y) \} \quad . \end{aligned} \quad (69)$$

where x_a and x_b are the coordinates of the boundary of the horn along the x-axis and $y_a(x)$ is the coordinate of the boundary along the y-axis, as shown in Figure 6.

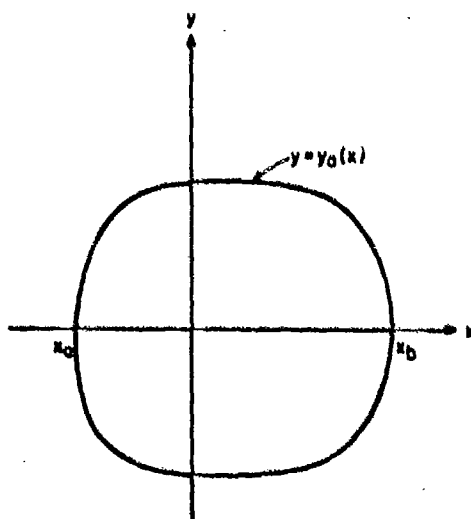


Figure 6. Projection of $z = f(x, y)$ onto the x-y Plane

Now, in the first integral in (69) we change y to $-y$ and use the fact that for $\phi = 0$ [Note that $\alpha_0(-y) = \alpha_0(y)$, $\beta_0(-y) = -\beta_0(y)$ and $\gamma_0(-y) = \gamma_0(y)$]

$$A_0(-y) = A_0(y) \quad , \quad (70)$$

$$B_0(-y) = -B_0(y) \quad , \quad (71)$$

$$C_0(-y) = C_0(y) \quad , \quad (72)$$

$$s_0(-y) = s_0(y) \quad , \quad (73)$$

$$g[\eta_0(-y)] = g[\eta_0(y)] \quad . \quad (74)$$

This gives

$$\left(\frac{2\pi R_0 e^{ikR_0}}{ikY_0} \right) \underline{H}_S = 2 \int_{x_a}^{x_b} dx \int_0^{y_a(x)} dy \frac{F(\psi_0) g(\eta_0)}{s_0} e^{-ik(s_0 - x \sin \theta - z \cos \theta)} \cdot \{ \hat{x} A_0(x, y) + \hat{z} C_0(x, y) \} \quad . \quad (75)$$

Also, from Eq. (62) we have that

$$A_0'''(-y) = A_0'''(y) \quad . \quad (76)$$

$$B_0'''(-y) = -B_0'''(y) \quad . \quad (77)$$

$$C_0'''(-y) = C_0'''(y) \quad . \quad (78)$$

Therefore, from Eq. (26) we get for the vacuum pattern

$$\frac{\pi^2 P_0(\theta)}{k^2 Y_0} = \left| \int_{x_a}^{x_b} dx \int_0^{y_a(x)} dy \frac{F(\psi_0) g(\eta_0)}{s_0} A_0 e^{-ikp_0} \right|^2 + \left| \int_{x_a}^{x_b} dx \int_0^{y_a(x)} dy \frac{F(\psi_0) g(\eta_0)}{s_0} C_0 e^{-ikp_0} \right|^2 \quad , \quad (79)$$

where

$$p_o = s_o - x \sin \theta - z \cos \theta .$$

Also, for the case of multipath and spherical Earth Eq. (58) becomes

$$\begin{aligned} \frac{\pi^2 P_{M0}(\theta)}{k^2 Y_o} = & \left| \int_{x_a}^{x_b} dx \int_0^{y_a(x)} dy \frac{F(\psi_o) g(\eta_o)}{s_o} e^{-iks_o} \left[A_o e^{i\xi_1} + A_o''' v e^{-i\xi_4} \right] \right|^2 \\ & + \left| \int_{x_a}^{x_b} dx \int_0^{y_a(x)} dy \frac{F(\psi_o) g(\eta_o)}{s_o} e^{-iks_o} \right. \\ & \cdot \left. \left[C_o e^{i\xi_1} + C_o''' v e^{-i\xi_4} \right] \right|^2 . \end{aligned} \quad (80)$$

The results $P_1[\theta(h)]$ and $P_{M1}[\theta(h)]$, which we would get for the case when the feed horn is located at $(x_1, 0, z_1)$ instead of $(x_o, 0, z_o)$, can be obtained from Eqs. (79) and (80) by replacing $\psi_o, \eta_o, p_o, s_o, A_o, C_o, A_o''', C_o'''$ by $\psi_1, \eta_1, p_1, s_1, A_1, C_1, A_1''', C_1'''$.

As a check on the validity of Eq. (80), we can consider the limit when $\delta = \psi_2 = 0$ (see Figure 7). In this case, we know that because the electric field is horizontally polarized, the power pattern at $\theta'' = -\theta$ should be zero. In this case, we find (for $a_e \rightarrow \infty$)

$$\begin{aligned} \theta_2 = \theta'' = -\theta , \\ p_2 = R_o , \\ \xi_4 = -\xi_1 , \\ A_o''' = -A_o , \\ C_o''' = -C_o , \\ v = 1 . \end{aligned} \quad (81)$$

So that upon using the results of Eq. (81) in (80) gives

$$P_{M0}(\theta = -\theta'' = -\theta_2) = 0 ,$$

as expected.

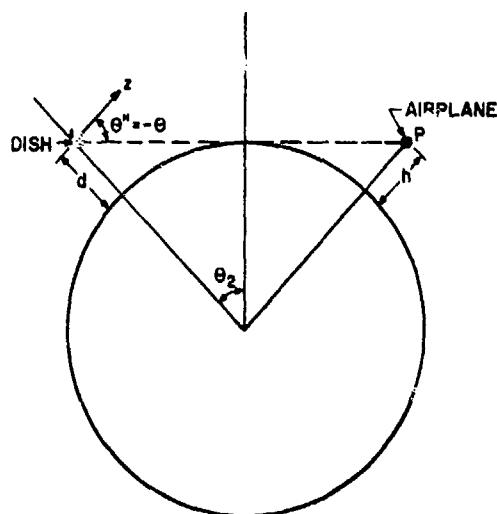


Figure 7. Limiting Case of Grazing Incidence.

5. FURTHER SIMPLIFICATION

If we now substitute for A_0 , C_0 , A_0''' , C_0''' etc. in Eqs. (79) and (80), we obtain the following simplified results:

$$\frac{\pi^2 P_0(\theta)}{k^2 Y_0} = |I_0(\theta)|^2 \quad (82)$$

$$\frac{\pi^2 P_{M0}(\theta)}{k^2 Y_0} = |I_0(\theta)|^2 + v^2 |I_0(-\theta''')|^2 \quad (83)$$

$$-2v \cos(\psi_2 + \theta_2 + \delta - \theta) \operatorname{Re}\{I_0(\theta) I_0^*(-\theta''') e^{ik\Delta R}\}$$

where

$$I_0(\theta) = \int_{x_a}^{x_b} dx \int_0^{y_a(x)} dy \frac{F(\psi_0) g(\eta_0)}{s_0} \left(s_0 + r_0 \frac{\partial f}{\partial x} \right) \quad (84)$$

$$\exp\{-ik(s_0 - x \sin \theta - z \cos \theta)\}$$

$$\Delta R = R_3 - R_0 = R_1 + R_2 - R_0 ,$$

and

Re denotes "real part of."

6. ERROR IN ALTITUDE DUE TO MULTIPATH

In the absence of multipath, it is possible to obtain information on an airplane altitude by placing two horns on the reflector system as shown in Figure 1, and then operating the system in a monopulse mode. In the absence of multipath, the voltage $V(h)$ (see Figure 1) is given by

$$\begin{aligned} V(h) &= K[\log P_1(h) - \log P_0(h)] \\ &= K \log \left[\frac{P_1(h)}{P_0(h)} \right] , \end{aligned} \quad (85)$$

where K is a constant, $P_1(h)$ is the power pattern due to the horn at $(x_1, 0, z_1)$, and $P_0(h)$ is the pattern (see Eq. 82) due to the horn at $(x_0, 0, z_0)$. A typical curve of V versus h (for a given airplane range r) is shown in Figure 1a. Now, because the measurement of V has some error ΔV in it, there is a corresponding error in our calculation of the airplane altitude h . This is indicated pictorially in Figure 1b.

The inclusion of multipath compounds our problem because now

$$V_M(h) = K \log \left[\frac{P_{M1}(h)}{P_{M0}(h)} \right] . \quad (86)$$

This leads to an additional error ΔV_M given by

$$\begin{aligned} \Delta V_M &= K \log \left[\frac{P_{M1}(h)}{P_{M0}(h)} \right] - K \log \left[\frac{P_1(h)}{P_0(h)} \right] \\ &= K \log \left[\frac{P_{M1}(h)}{P_1(h)} \cdot \frac{P_0(h)}{P_{M0}(h)} \right] . \end{aligned} \quad (87)$$

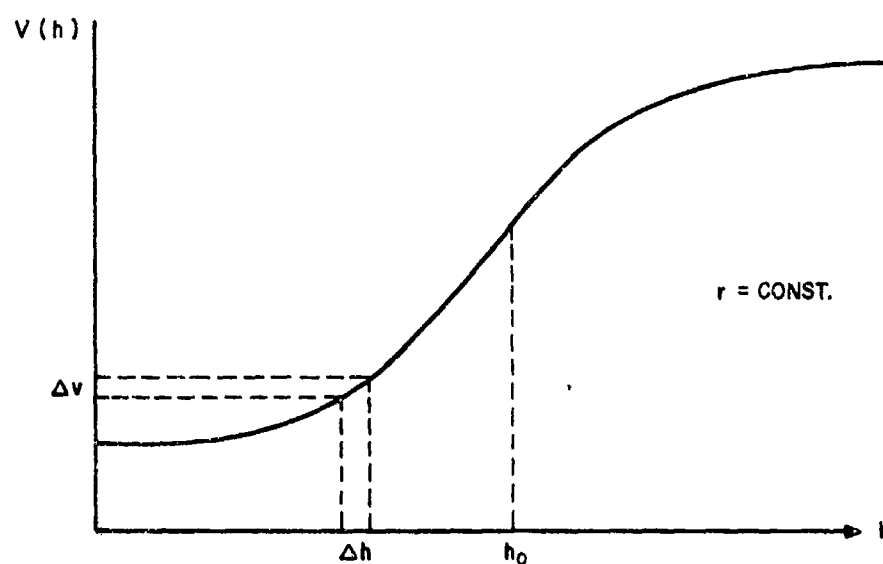


Figure 8a. Plot of Output Voltage V Versus Target Altitude h in the Absence of Multipath, Showing How Measurement Error ΔV Leads to Altitude Error Δh

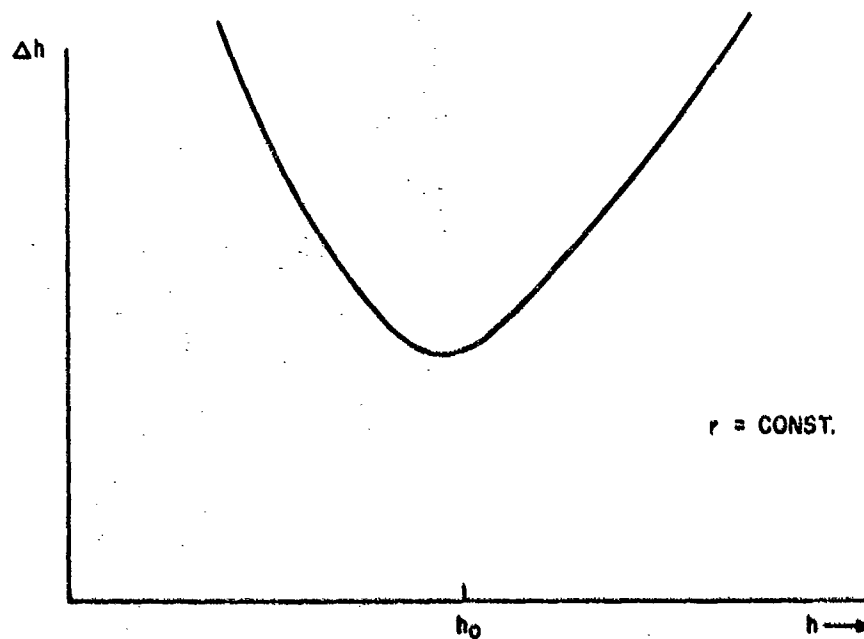


Figure 8b. Typical Plot of Altitude Error When Multipath is Absent

A typical measurement of $V_M(h)$ is shown in Figure 9a for a fixed target range r . The envelope of ΔV_M is also indicated on Figure 9a. Let us suppose that the error for a given h , say h_1 , is $\Delta V_M(h_1)$. We then plot this error on Figure 8a to obtain the result shown in Figure 9b. By using Figure 9b, it is possible to calculate curves of the error Δh (due to multipath) in altitude versus altitude h for a number of different target ranges. A typical result is shown in Figure 10a. It is often convenient to plot the results in Figure 10a versus range with altitude as a parameter; a typical result is shown in Figure 10b.

In part 2 of this report, we will employ Eqs. (82) and (83), etc., to present curves of the error in altitude Δh versus h and r for specific radar configurations.

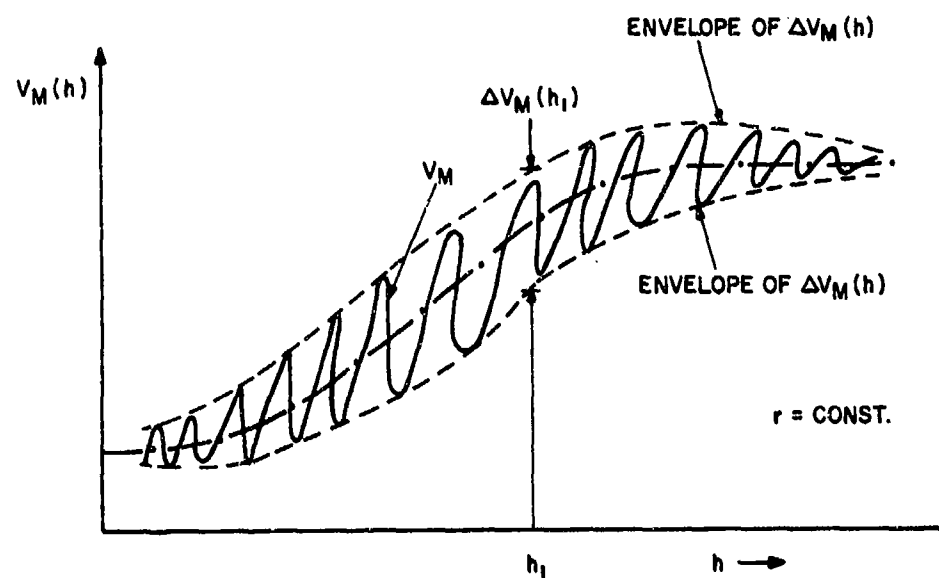


Figure 9a. Plot of Output Voltage V_M Versus h When Multipath is Included

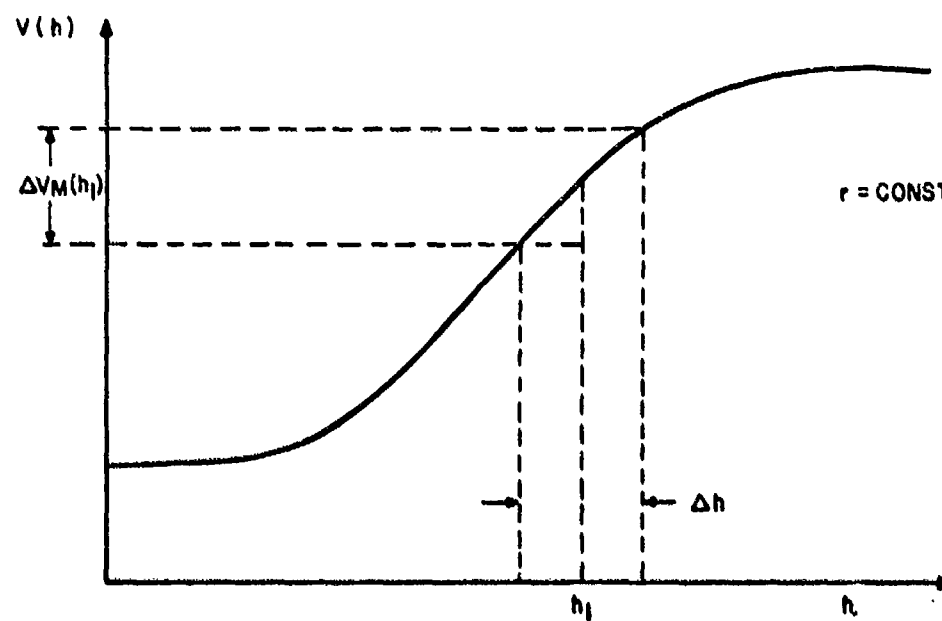


Figure 9b. An Indication of How ΔV_M can be Used to Get Airplane Height Error Δh

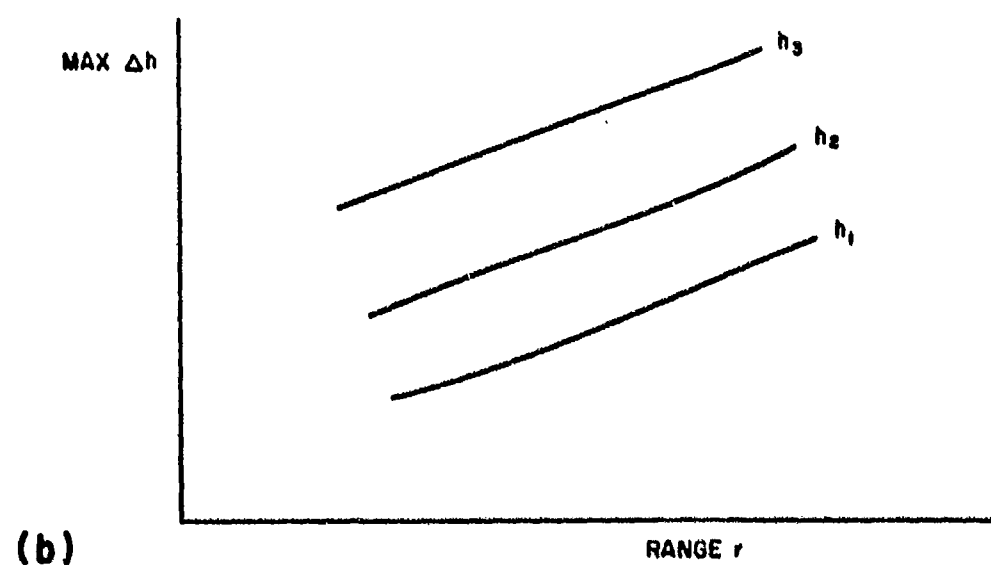
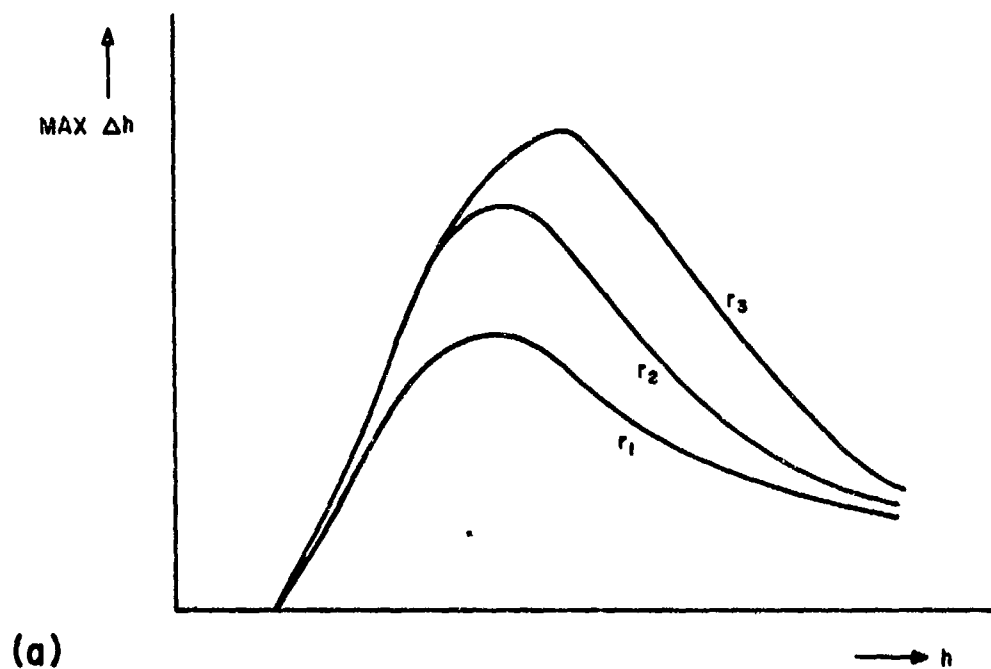


Figure 10. Typical Plots of Maximum Altitude Error Versus (a) Airplane Altitude and (b) Airplane Range